DOI: 10.1002/ejic.200800621

Metallocenium Salts of Nickel Bis(α-thiophenedithiolate) $[M(Cp^*)_2][Ni(\alpha\text{-tpdt})_2]$ (M = Fe, Mn, Cr) – Metamagnetism and Magnetic Frustration

Dulce Belo,[a] Joana Mendonça,[a] Isabel C. Santos,[a] Laura Cristina Jesus Pereira,[a] Manuel Almeida,*[a] Juan J. Novoa,[b] Concepció Rovira,[c] Jaume Veciana,[c] and Vasco Gama*[a]

Keywords: Donor–acceptor systems / Metallocenes / S ligands / Through-space interactions / Magnetic anisotropy

The family of charge-transfer (CT) salts $[M(Cp^*)_2][Ni(\alpha\text{-tpdt})_2]$ [α-tpdt = 2,3-thiophenedithiolate; M = Fe (**1**), Mn (**2**), Cr (**3**)] were prepared. The crystal structure of **3** is similar to that previously reported for **1** and is composed of alternating layers each consisting of parallel mixed donor–acceptor $D^+A^-D^+A^-D^+A^-$ chains, and the chains in adjacent layers are perpendicular. A similar crystal structure is expected to occur in **2**. The McConnell I model was used to analyze the intermolecular magnetic coupling in this family of compounds. The predicted ferromagnetic (FM) intrachain coupling and the antiferromagnetic (AFM) coupling in the interchain coupling (both intra and interlayer) are in good agreement with the experimental results. The magnetic behavior of these compounds is dominated by FM interactions, which are ascribed to the intrachain FM DA interactions. The low-temperature magnetic behavior of the new CT salts contrasts that previously reported for metamagnetic compound **1**. Whereas CT salt **3** remains paramagnetic down to 1.6 K, **2** shows magnetic behavior that is typical of a frustrated magnet and has a blocking temperature of ca. 4 K. For this compound, the magnetic frustration results from a degenerate ground state in the interlayer spin arrangements.

Introduction

Within continued efforts in our group to explore new transition-metal bisdithiolene complexes based on extended conjugated ligands, we previously described a new series of coordination complexes based on thiophenedithiolate ligands. The first studies were concentrated on Au[1] and Ni[2] complexes, which were generally characterized by rather low oxidation potentials, which were often obtained in their neutral state. This tendency was also observed in the corresponding Cu, Co, and Pt complexes.[3] Recently, a series of $[Ni(\alpha\text{-tpdt})_2]^-$ (α-tpdt = 2,3-thiophenedithiolate) salts with differently substituted benzyl pyridinium cations were prepared, and they showed magnetic behavior that was sensitive to variable degrees of *cis–trans* disorder in the anions.[4]

The $S = 1/2$ $[Ni(\alpha\text{-tpdt})_2]^-$ (A^-) complex was recognized as a suitable radical anion to be used as a building block to obtain new molecular magnetic materials when combined with the $S = 1/2$ $[Fe(Cp^*)_2]^+$ (D^+) cation, thus forming the $[Fe(Cp^*)_2][Ni(\alpha\text{-tpdt})_2]$ (**1**) charge-transfer (CT) salt. The crystals present a peculiar structure consisting of alternating layers, each composed by parallel $D^+A^-D^+A^-$ chains, where the chains in adjacent layers are nearly perpendicular. This compound displays an interesting metamagnetic behavior with T_N = ca. 2.5 K and a critical field of ca. 600 G at 1.7 K.[2]

Here we report the structure and magnetic properties of the $[M(Cp^*)_2][Ni(\alpha\text{-tpdt})_2]$ CT salts obtained with two new radical cations: $S = 1$ $[Mn(Cp^*)_2]^+$ (**2**) and $S = 3/2$ $[Cr(Cp^*)_2]^+$ (**3**). The three salts are expected to present similar crystal structures; therefore, the effects from the spin value and the magnetic anisotropy of the cations can be studied. The intermolecular magnetic coupling was analyzed by using the McConnell I mechanism in its more strict form,[5] and the crystal structure and the intermolecular magnetic coupling were correlated with the magnetic behavior of these compounds.

Results and Discussion

Synthesis

Compounds **2** and **3** were obtained by slow addition of concentrated acetonitrile solutions of $[Mn(Cp^*)_2]PF_6$[6] and $[Cr(Cp^*)_2]PF_6$[7] to stoichiometric amounts of concentrated

[a] Depart. Química, Instituto Tecnológico e Nuclear/CFMCUL, Estrada Nacional 10, 2686-953 Sacavém, Portugal
Fax: +351-219941455
E-mail: vascog@itn.pt
[b] Depart. Quimica Fisica, Fac. Quimica & IQTCUB, Universitat de Barcelona,
Av. Diagonal 647, 08028 Barcelona, Spain
[c] Institut de Ciència des Materials de Barcelona (CSIC), Campus Universitari de Bellaterra, 08193 Cerdanyola, Spain
Supporting information for this article is available on the WWW under http://www.eurjic.org or from the author.

acetonitrile solutions of nBu$_4$N[Ni(α-tpdt)$_2$],[2] under strictly anaerobic and dry conditions. Polycrystalline precipitates were collected by vacuum filtration. In case of **3**, single crystals suitable for X-ray diffraction were isolated from the collected precipitates. No single crystals of **2** suitable for X-ray analysis could be obtained from the obtained microcrystalline powder. Further, attempts to crystallize the compounds (with a variety of solvents) were unsuccessful, leading frequently to partial decomposition.

Crystal Structure

In the crystal structure of [Cr(Cp*)$_2$][Ni(α-tpdt)$_2$] (**3**) the unit cell contains one independent [Ni(α-tpdt)$_2$]$^-$ anion and one independent [Cr(Cp*)$_2$]$^+$ cation, where both the Cr and the Ni atoms are located at inversion centers. The [Cr(Cp*)$_2$]$^+$ units adopt the geometry typical of the metallocenium cations with a staggered configuration. Within experimental error, the [Ni(α-tpdt)$_2$]$^-$ anion is planar (rms deviation of fitted atoms = 0.0127 Å) and presents only a *trans* configuration, as in [Fe(Cp*)$_2$][Ni(α-tpdt)$_2$] (**1**). The Ni–S bond lengths observed in this Ni complex, with an average value of 2.164(.2) Å, are identical to those previously found in the [Ni(α-tpdt)$_2$]$^-$ anion[2,4] and correspond to the typical distances observed in Ni^{III} dithiolates.[8,9]

Compounds **1** and **3**, although not strictly isostructural, present a similar supramolecular packing. The crystal structure of **3** consists of alternating layers composed of parallel alternating ···D$^+$A$^-$D$^+$A$^-$D$^+$A$^-$··· chains. In this multilayer structure, the chains in adjacent layers are perpendicular, alternatively aligned either along the [1 –1 0] direction (A layers) or along the [1 1 0] direction (B layers), as illustrated for **3** in Figure 1a.

No contacts shorter than the sum of the van der Waals radii (d_W) were detected in the structure. However, relatively short D$^+$A$^-$ separations were observed within the chains, where the thiophenic rings (C$_4$S) of the anions sit on top of the cyclopentadienyl rings (C$_5$) of the cations, denoting significant π–π intrachain interaction. The closest D$^+$A$^-$ separation of this type (d = 3.576 Å, represented by the dashed lines in Figure 1), corresponds to the S3···C8 contact, exceeding d_W by 2%. Other slightly larger D$^+$A$^-$ π–π (C···C) contacts were observed, and the D$^+$A$^-$ separations exceed d_W by ca. 5–10%. Both cation and anion molecules are considerably tilted in relation to the chain axis (tilting angles of 32.24 and 42.15°, respectively). Figure 1b shows a view of the A and B layers (left and right, respectively) along the [1 0 2] direction. The chains in these layers present an out-of-registry arrangement and relatively short D$^+$A$^-$ interchain contacts were observed involving the S1 atom of a MS$_4$ fragment from the [Ni(α-tpdt)$_2$]$^-$ anions and the C81 atom of a methyl group from the [Cr(Cp*)$_2$]$^+$ cations; the interatomic separation of 3.615 Å exceeds d_W by ca. 3%. These interchain intralayer contacts are represented by the thin dashed lines in Figure 1b. The angle between the cations in adjacent layers is of 67.98°, whereas for the anions the angle is 67.75°.

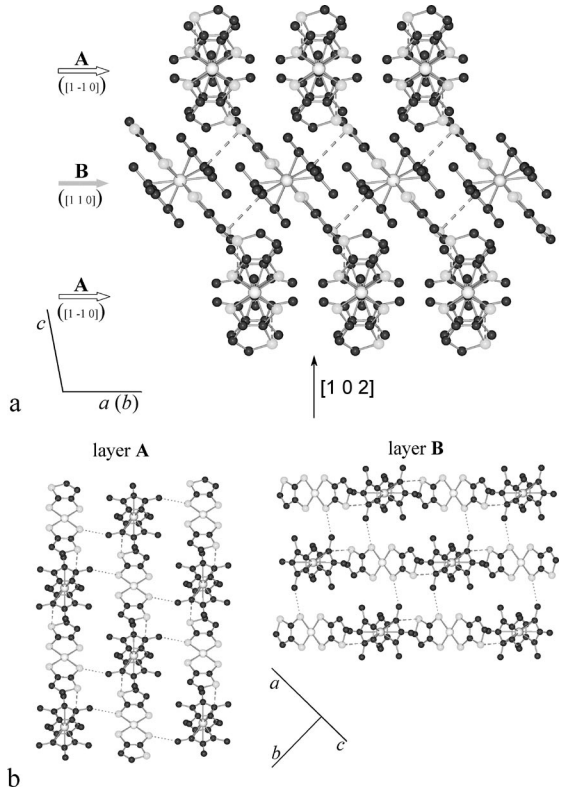

Figure 1. (a) View of the crystal structure of **3** along the [1 –1 0] direction; the shortest intrachain D$^+$A$^-$ contacts are represented by dashed lines; (b) view of the A (left) and B (right) chain layers along the [1 0 2] direction. For clarity, the H atoms were omitted.

The perpendicular chains in neighboring layers are connected by relatively short A$^-$A$^-$ contacts involving the S1 atom from the central NiS$_4$ fragment and the C3 atom from the C$_4$S ring; the S···C separations of 3.701 Å exceed d_W by ca. 6%. The anions connecting the neighboring chain layers are organized as sheets parallel to the *bc* plane, as illustrated in Figure 2. In this figure, anions from three consecutive chain layers (ABA) are shown and the A$^-$A$^-$ contacts are represented by dashed lines. The cations present short H61B···H71A contacts, and their separation d = 2.440 Å slightly exceeds d_W by 2%; the separation between the C atoms of the two Me groups (C61 and C71) is 3.970 Å, which exceeds d_W by ca. 17%.

Compound **1** presents a similar multilayer (ABAB) supramolecular arrangement to that of **3**; a doubling of the cell axis is associated with alternations in intra- and interchain contacts in **1** (the intrachain arrangements of **3** and **1** are shown in Figure S1 in the Supporting Information). The interchain interlayer (S–C) A$^-$A$^-$ contacts present a slight distinct arrangement. For **3**, the contacts between one anion and two neighbors located in an adjacent layer are similar, whereas for **1** one of those contacts is shorter (Figure S2 in the Supporting Information).

The poor quality of the crystals of **2** prevented its crystal structure determination. However, a structure similar to that observed for **3** is expected as indicated by the powder X-ray diffraction pattern.

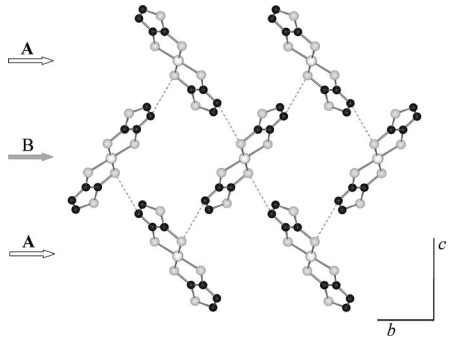

Figure 2. View of the anion arrangements connecting three consecutive chain layers (ABA). The shorter A$^-$A$^-$ contacts are represented by dashed lines.

Magnetic Properties

Nature of the Magnetic Interactions in Salts 1–3

The χT (χ is the molar magnetic susceptibility) product temperature dependence of salts **1**–**3** is shown in Figure 3. At high temperatures, the increase in χT upon cooling indicates dominant ferromagnetic (FM) interactions in these compounds. For $T > 30$ K, the paramagnetic susceptibility follows a Curie–Weiss behavior: $\chi = C/(T - \theta)$, with θ values of 3.8, 7.5, and 3.0 K for **1**, **2**, and **3**, respectively. As reported earlier,[2] for the two related compounds [Co(Cp*)$_2$][Ni(α-tpdt)$_2$] (**4**) and [Fe(Cp*)$_2$][Au(α-tpdt)$_2$] (**5**) (where in the first the cation is diamagnetic, $S_D = 0$ and $S_A = 1/2$, and in the second the anion is diamagnetic, $S_D = 1/2$ and $S_A = 0$) the dominant interactions were found to be antiferromagnetic (AFM). Compounds **1** and **4** are isostructural, and although the crystal structure of **5** was not determined, a similar structure is expected for this salt.

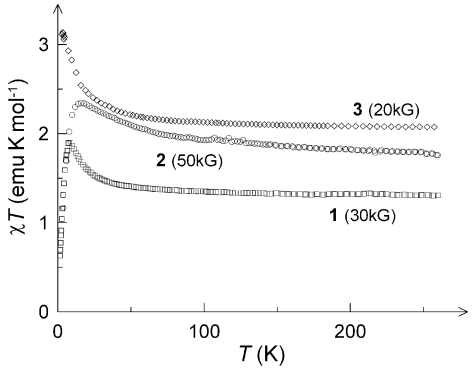

Figure 3. χT temperature dependence for **1** (squares), **2** (circles) and **3** (diamonds).

In order to rationalize the nature of the magnetic interactions in these crystals, qualitative comparative analysis based on the McConnell I mechanism was performed,[5] as the number and complexity of these crystals, together with the size of the radicals, precluded quantitative analysis. Although the validity of this mechanism has been questioned both theoretically[10] and experimentally,[11] this mechanism was shown to work in cases of high symmetry owing to error compensations. It is also expected to work in comparative studies of isostructural crystals, where the errors introduced are similar. In the most common use of the McConnell I mechanism, the nature of the magnetic intermolecular coupling is determined by the sign of the spin density (ρ^S) of the atoms involved in the shortest intermolecular contact between the two interacting radicals: AFM coupling is predicted when both atoms present the same sign of ρ^S and FM coupling is predicted when the atoms have different signs of ρ^S. It should be noted that the use of the McConnell I mechanism is a simplification to one component of the original expression proposed by McConnell, where all short contacts among pairs of atoms of the two interacting radicals were considered. Hereafter, we will see that when the usual simplified form of McConnell I is used (only one short contact per radical pairs) the mechanism does not predict the proper sign for the interaction; it does, however, provide a proper description when all the relevant short distances are included.

In the case of the [Fe(Cp*)$_2$]$^+$ cation, B3LYP/LANL2DZ calculations indicate that the spin density mostly resides on the Fe atom, although a spin polarization effect was observed in the C_5Me_5 ligands. This can be numerically illustrated by looking at the atomic population, ρ^S,[12] $\rho_{Fe} = 1.26$ a.u., which is in agreement with NMR spectroscopic[13] and neutron diffraction[14] studies. A spin polarization effect was observed in the C_5Me_5 ligands, where the carbon atoms of the Cp ring have a negative ρ^S value ($\rho_C = -0.03$ a.u.) and the C atoms from the methyl groups (C′) show a small positive ρ^S value ($\rho_{C'} = 0.002$ a.u.). The value of ρ^S for the methyl H atoms is negligible, ($|\rho_H| < 0.002$ a.u.). A similar spin distribution is expected for the [M(Cp*)$_2$]$^+$ (M = Mn and Cr) cations.[13,14] In case of the [Ni(α-tpdt)$_2$]$^-$ anion, its atomic ρ^S distribution is represented in Figure 4. Although most of the ρ^S (>85%) is located in the central NiS_4 fragment of the anion, a significant contribution was found to extend along the ligands in the peripheral thiophenic rings. A spin polarization effect was observed in the α-tpdt ligands, where the S and C atoms connected to the ethylene C atoms present a negative ρ^S value. Also, a nonnegligible ρ^S value was observed in the terminal H atoms. The populations for the cation and the anion were computed by performing a Mulliken population analysis on the wavefunction obtained by B3LYP density functional[15] computations with the LANL2DZ basis set,[16] which uses pseudopotentials for the core electrons and a double-zeta basis set for the valence electrons. In these calculations, the geometry of the anion was found in the crystal without further changes. The ground state is a doublet and the spin contamination in the B3LYP wavefunction was very small.

In the qualitative analysis of the intermolecular magnetic coupling done hereafter, two main factors were considered (i) the interatomic separations, measured by using the parameter $q = d/d_W$, which gives more information than the interatomic separation d and (ii) the product of the ρ^S of the atoms involved in the contacts. In cases where several contacts must be considered, a semiquantitive evaluation of

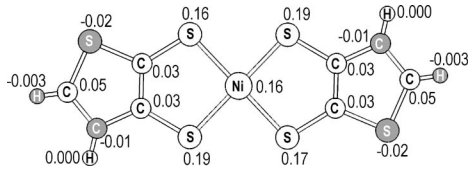

Figure 4. Atomic ρ^S distribution in the $[Ni(\alpha\text{-tpdt})_2]^-$ anion. The atoms exhibiting a negative ρ^S are represented by dark circles, whereas those with a positive ρ^S are represented by open circles.

the contributions from the different contacts will be made through a coupling parameter that considers both factors, $\phi_{ij} = \rho^S{}_i\rho^S{}_j/q_{ij}{}^3$.

D^+D^+ Interactions

The shortest contacts between cations involve the methyl groups. They generate various short-distance through-space contacts (H···H, C···H, C···C). According to the calculations, the value of ρ_H is very small ($|\rho_H| < 0.002$), and after considering the spin distribution in the Fe and C atoms, the residual spin density (0.02) must be distributed among the 30 H atoms to give an average value of ρ_H of ca. 0.0007. The signal of ρ_H for each H atom is unknown, but we will consider a limit value for $|\rho_H|$ of 0.001. For compounds **1** and **3**, the obtained values for $|\phi_{HH}|$ are 7.97×10^{-7} and 9.52×10^{-7}, respectively, and $|\phi_{CH}| = 1.56\times10^{-6}$ and 1.53×10^{-6}, respectively. In case of C···C contacts, $\phi_{CC} = 2.98\times10^{-6}$ and 2.51×10^{-6} for **1** and **3**, respectively. The through-space C···C contacts seem to be dominant, as ϕ_{CC} is considerably larger than $|\phi_{HH}|$ and $|\phi_{CH}|$; furthermore, its positive value indicates that the D^+D^+ coupling must be AFM. This is in good agreement with the dominant AFM interactions observed in **5**, where the only spins present are associated with the $S = 1/2$ $[Fe(Cp^*)_2]^+$ cations.

A^-A^- Interactions

A detailed view of the interlayer anion–anion (A^-A^-) contacts is shown in Figure 5. The anions A_i and A_{ii} belong to adjacent chains of the same layer, whereas A_{iii} belongs to a neighboring layer. The S···C distances of the contacts presented in Figure 5, as well as the ρ^S values of the C atoms involved in those contacts, for compounds **1** and **3** are summarized in Table 2. In the two pairs of anions (A_i/A_{iii} and A_{ii}/A_{iii}) a competition between FM (1a and 2a) and AFM (1b and 2b) contacts is observed. As indicated by the ϕ_{SC} values presented in Table 1, despite being slightly longer, the AFM interactions are expected to be dominant, as the ρ^S value for the C atoms involved in these contacts ($\rho_C = 0.05$) is significantly larger than that in the FM contacts ($\rho_C = -0.01$). Therefore, for compounds **1** and **3** the A^-A^- magnetic coupling is expected to be AFM, which is in good agreement with the AFM interactions observed in **4**, where the only spins present are associated with the $S = 1/2$ $[Ni(\alpha\text{-tpdt})_2]^-$ anions.

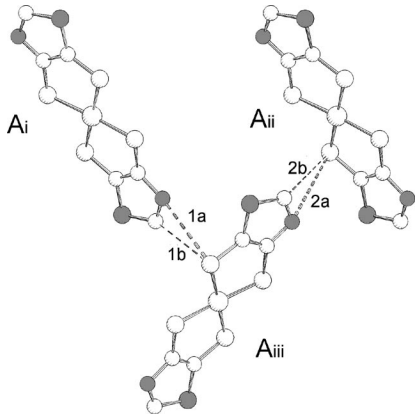

Figure 5. Schematic representation of the interchain interlayer arrangement between three anions, where A_i and A_{ii} belong to neighboring chains in one layer and A_{iii} to a chain in an adjacent layer for compounds **1** and **3**. The shortest A^-A^- contacts are represented by dashed lines. The atoms with $\rho^S < 0$ are darker than those with $\rho^S > 0$.

Table 1. Summary of the S···C A^-A^- contacts in compounds **1** and **3**.

$[Fe(Cp^*)_2][Ni(\alpha\text{-tpdt})_2]$				
Contact[a]	d_{SC} (Å)	q_{SC}[b]	ρ_C[c]	Int.[d] ($\lvert\phi_{SC}\rvert$[e])
1a	3.723	1.06	–0.01	FM (1.37×10^{-3})
1b	3.805	1.09	0.05	AFM (6.42×10^{-3})
2a	3.751	1.07	–0.01	FM (1.34×10^{-3})
2b	3.798	1.09	0.05	AFM (6.46×10^{-3})
$[Cr(Cp^*)_2][Ni(\alpha\text{-tpdt})_2]$				
Contact[a]	d_{SC} (Å)	q_{SC}[b]	ρ_C[c]	Int.[d] ($\lvert\phi_{SC}\rvert$[e])
1a = 2a	3.701	1.06	–0.01	FM (1.40×10^{-3})
1b = 2b	3.762	1.07	0.05	AFM (6.64×10^{-3})

[a] S···C A^-A^- contacts in **1** and **3** (see Figure 5). [b] $q_{SC} = d_{SC}/d_W$. [c] The ρ_C values of the C atoms involved in the contacts. [d] Nature of the coupling as predicted by the McConnell I model. [e] $\phi_{SC} = \rho_S\rho_C/q_{SC}{}^3$ ($\rho_S = 0.16$).

D^+A^- Interactions

In the crystal structures of compounds **1** and **3**, two types of cation–anion (D^+A^-) contacts were observed: the intra- and interchain contacts within the same layers. In **1**, two D^+A^- intrachain overlap modes were observed, as illustrated in Figure 6 (top). Both involve the Cp* rings of the cations and the thiophenic fragments of the anions (C_4S). In **3**, only one overlap mode between the cation Cp rings and the anion C_4S rings was observed, as shown in Figure 6 (bottom). In the D^+A^- intrachain contacts of compounds **1** and **3**, there are overlapping atoms where both carry a negative ρ^S value (unshaded regions), which must give rise to AFM coupling; these coexist with overlapping atoms that present ρ^S values with opposite signs (shaded regions) that are expected to lead to FM coupling. The intrachain D^+A^- distances of the contacts shown in Figure 6, as well as the ρ^S values of the anion atoms involved in those contacts, are summarized in Table 2. The D^+A^- magnetic coupling must be dominated by FM contacts, because in addition to involving a larger number of contacts, the ρ^S val-

ues of the atoms from the C_4S ring atoms in these contacts are considerably larger than those involved in the AFM D^+A^- contacts.

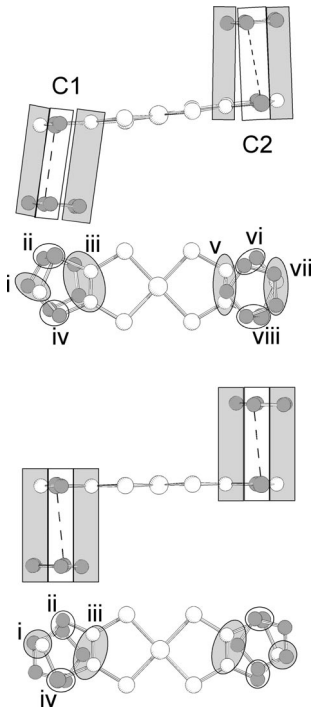

Figure 6. Side view and top view of the overlap modes between the Cp rings of the cations and the thiophenic groups of the anions in **1** (top) and **3** (bottom). The atoms with $\rho^S > 0$ are represented by open circles and those with $\rho^S < 0$ are represented by closed circles. The FM contacts are represented by shaded areas and the AFM contacts are represented by unshaded areas.

In compounds **1** and **3**, the shortest D^+A^- interchain contacts involve C and H atoms from the methyl groups of the cations and coordinating S atoms of the anions. Although the shorter interatomic contacts correspond to S···H contacts, the slightly longer S···C trough-space contacts are expected to be determinant in the interchain as a result of the much larger spin population on the C atom relative to that on the H atom. The values obtained for $|\phi_{SH}|$ are 1.79×10^{-4} and 1.49×10^{-4} for **1** and **3**, respectively, and $\phi_{SC} = 4.30 \times 10^{-4}$ and 4.49×10^{-4} for **1** and **3**, respectively. As both atoms involved in the S···C contacts present positive ρ^S values, the interchain intralayer D^+A^- interactions are expected to be AFM.

The analysis of the intermolecular contacts according to the McConnell I model in salts **1** and **3** showed that the dominant FM interactions observed in compounds **1**, **3**, and **2** (isostructural with **3**) can be attributed to the D^+A^- intrachain contacts. AFM interactions, associated with intralayer interchain D^+A^- contacts, as well as with D^+D^+ and A^-A^- interlayer contacts, were observed to coexist with the stronger intrachain FM D^+A^- contacts. This type of magnetic anisotropy seems to be in good agreement with the metamagnetic behavior exhibited by **1**,[2] as described in detail further down. The AFM nature of the A^-A^- and D^+D^+ interactions is consistent with the magnetic behavior shown by analogous CT salts **4** and **5**, where $S = 0$, either for the cation or the anion species.

Table 2. Summary of the D^+A^- intrachain contacts in compounds **1** and **3**.

	[Fe(Cp*)$_2$][Ni(α-tpdt)$_2$]				
	Contact[a]	d_{Cj} (Å)	q_{Cj}[b]	ρ_j[c]	Int.[d] ($\|\phi_{Cj}\|$[e])
i	C–C	3.479	1.02	0.05	FM (1.40×10^{-3})
ii	C–S	3.529	1.01	–0.02	AFM (5.85×10^{-4})
iii	C–C	3.766	1.11	0.03	FM (6.62×10^{-4})
	C–C	3.759	1.11	0.03	FM (6.66×10^{-4})
iv	C–C	3.577	1.05	–0.01	AFM (2.58×10^{-4})
v	C–C	3.714	1.09	0.03	FM (6.90×10^{-4})
	C–C	3.700	1.09	0.03	FM (6.98×10^{-4})
vi	C–C	3.532	1.04	–0.01	AFM (2.68×10^{-4})
vii	C–C	3.583	1.05	0.05	FM (1.28×10^{-3})
	C–C	3.686	1.08	0.05	FM (1.18×10^{-3})
viii	C–S	3.609	1.03	–0.02	AFM (5.47×10^{-4})
	[Cr(Cp*)$_2$][Ni(α-tpdt)$_2$]				
	Contact[a]	d_{Cj} (Å)	q_{Cj}[b]	ρ_j[c]	Int.[d] ($\|\phi_{Cj}\|$[e])
i	C–C	3.587	1.06	0.05	FM (1.28×10^{-3})
ii	C–C	3.619	1.06	–0.01	AFM (2.49×10^{-4})
iii	C–C	3.747	1.10	0.03	FM (6.72×10^{-4})
	C–C	3.662	1.08	0.03	FM (7.20×10^{-4})
iv	C–S	3.576	1.02	–0.02	AFM (5.63×10^{-4})

[a] D^+A^- intrachain contacts in **1** and **3** (see Figure 6). [b] $q_{Cj} = d_{Cj}/d_W$. [c] The ρ_j values of the anion atoms involved in the contacts. [d] Nature of the coupling as predicted by the McConnell I model. [e] $\phi_{Cj} = \rho_C\rho_j/q_{Cj}^3$ ($\rho_C = -0.03$).

Low-Temperature Magnetic Behavior of Salts 1–3

In spite of the similarities observed in both the crystal structures and the magnetic intermolecular couplings of salts **1**–**3**, the low-temperature magnetic behaviors exhibited by these compounds are quite different. Compound **3** remains a paramagnet down to 1.6 K, **1** exhibits metamagnetic behavior (with $T_N = 2.5$ K), whereas in **2**, a slow relaxation of the magnetization was observed below ca. 4 K. This change in macroscopic magnetic behavior is analyzed in detail hereafter.

Magnetic Behavior of [Fe(Cp)$_2$][Ni(α-tpdt)$_2$] (1)*

As previously reported, **1** exhibits metamagnetism.[2] For low applied magnetic fields, the magnetization temperature dependence shows a maximum corresponding to a transition to an AFM ground state. However, the application of a high magnetic field (≈800 G) suppresses this transition. Below $T_N = 2.5$ K, at low applied magnetic fields the magnetization isothermals exhibit sigmoidal behavior, typical of a metamagnet (low-temperature magnetization isofield and isothermal measurements of **1** are presented in Figure S3 in the Supporting Information).

The metamagnetic behavior of compound **1** can be attributed to the AFM coupling between the FM coupled $D^+A^-D^+A^-$ chains within the chain layers, as described in the previous section. This is similar to other metamagnetic CT salts also based on decamethylmetallocenes and on

planar transition-metal bisdichalcogenate complexes[12,17], where the crystal structure consists of arrangements of parallel alternating mixed chains. According to application of the McConnell I model, the metamagnetism in those salts results from the coexistence of strong D^+A^- FM intrachain coupling and weaker (A^-A^- or D^+A^-) AFM interchain interactions.[12,17b] In this context, it is worthwhile to note that the interchain intralayer AFM D^+A^- contacts observed in **1** are similar to those reported for the metamagnets $[Mn(Cp^*)_2][M(tdt)_2]$ (M = Ni, Pd, Pt).[12,17c]

Magnetic Behavior of [Mn(Cp)$_2$][Ni(α-tpdt)$_2$] (2)*

As in the case of **1**, a metamagnetic behavior could be anticipated for **2**, as both compounds are expected to exhibit similar crystal structures and magnetic anisotropies. However, no AFM phase transition could be detected in **2**, even with rather low applied magnetic fields (H = 5 G). This can be attributed to (i) a significant decrease in the AFM interchain intralayer coupling or (ii) a change in the nature of the interchain magnetic coupling. The first situation (i) would imply considerably weaker D^+A^- interchain intralayer interactions. The second situation (ii) could result from FM interchain intralayer coupling induced by superexchange interactions through the A^-A^- contacts involving anions in neighboring layers (Figure 7), where the A^-A^- interactions are represented for compounds **1** (left) and **2** (right) by assuming that these compounds have similar crystal structures. For both compounds the interchain coupling is expected to be AFM due to the D^+A^- interchain interactions ($J_{iCh} < 0$). As illustrated for compound **2** in Figure 7 (right), when the AFM A^-A^- interlayer interactions (J_{iL}) are strong enough, these interactions can overcome J_{iCh} and lead to an FM interchain intralayer arrangement. A distinct situation seems to occur in **1**, as schematically represented in Figure 7 (left), where the AFM A^-A^- interlayer interactions (J_{iL}) are not strong enough to overcome J_{iCh}, and the intralayer interchain AFM arrangement is more stable at low applied magnetic fields.

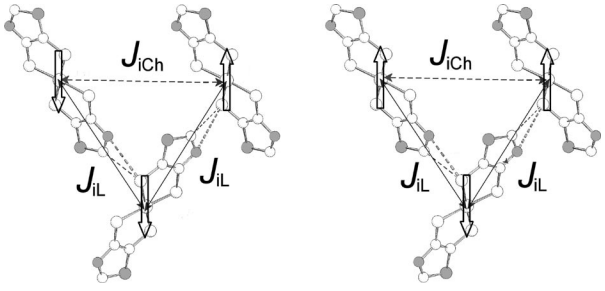

Figure 7. Schematic representation of the effective interchain intralayer magnetic couplings for compounds **1** (left) and **2** (right) as a result of the interchain intra- and interlayer coupling, J_{iCh} and J_{iL}.

The field-cooled (FC) and zero-field-cooled (ZFC) direct current (dc) magnetization (M^{FC} and M^{ZFC}) temperature dependences with an applied field of 100 G for compound **2** are shown in Figure 8. At low temperatures ($T < 4$ K), small differences between the FC and the ZFC magnetization measurements were detected. From 1.6 to 2 K, M^{FC} is slightly larger than M^{ZFC}, and above 2 K, M^{ZFC} becomes slightly larger than M^{FC}; at ca. 4 K this difference seems to vanish and for higher temperatures the two curves overlap. This slight difference between M^{FC} and M^{ZFC} was consistently observed in measurements from 5 to 300 G, but for higher fields it was no longer detected. The temperature dependence of the remnant magnetization (REM) with an applied field of 100 G is also shown in Figure 8. REM is negative and increases upon warming. This increase is quite drastic at $T < 1.85$ K. For higher temperatures the increase is more gradual and approaches zero slowly, and at ca. 4 K the obtained REM value is within the margin error of the measurement. The negative REM is associated with an unusual inverted hysteresis detected in magnetization isothermals of this compound that will be described in detail elsewhere.[18] At low temperatures, the magnetization temperature dependence of compound **2** suggests the existence of an "ordering process" occurring at ca. 3–4 K.

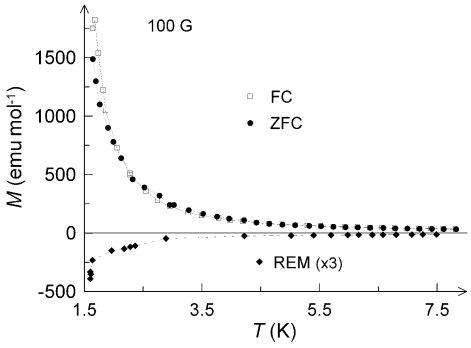

Figure 8. Temperature dependence of M^{ZFC} (circles), M^{FC} (squares), and REM (diamonds) of compound **2**, with an applied field of 100 G.

The isothermal obtained at 1.65 K for **2** is shown in Figure 9. At low applied magnetic fields ($H < 1$ kG), the magnetization increases drastically and much faster than that predicted by the Brillouin function (solid line). For high fields ($H > 10$ kG), the magnetization increase is much more gradual and it does not saturate up to 120 kG, where it attains a value of ca. 3 $N\mu_B$, which is still smaller than the calculated saturation magnetization (3.3 $N\mu_B$) for S_A = 1/2, S_D = 1, g_A = 2.06,[2] and g_D = 2.2.[6]

Although the direct current (dc) magnetic susceptibility (χ_{dc}) in both FC and ZFC measurements increase monotonically upon cooling, as in a simple paramagnet with no magnetic ordering or spin freezing, the "ordering process" suggested by the remnant magnetization was also clearly revealed by the alternating current (ac) susceptibility (χ_{ac}) measurements with polycrystalline samples of **2**, as shown in Figure 10. Below 4 K, the real (χ') and imaginary (χ'') components of the ac susceptibility showed a strong frequency dependence, which precludes any tridimensional ordering and indicates a spin-freezing process into a nonequilibrium state. A similar slow relaxation of the magnetization was observed in spin-glass-like materials,[19] superparamag-

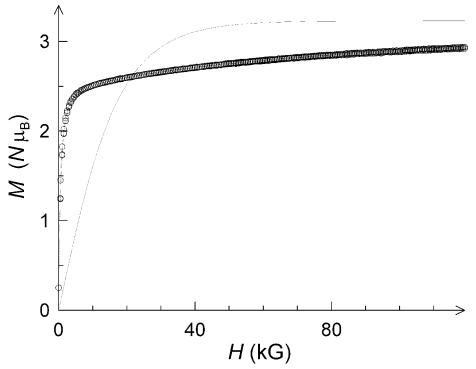

Figure 9. Magnetization field dependence at 1.65 K for **2**; the solid line represents the calculated values from the Brillouin function.

nets (SP),[19,20] single-molecule magnets (SMM),[21] single-chain magnets (SCM),[22] and highly frustrated magnets.[23] With cooling, the dynamic response of the spin slowed down, and below the freezing temperature (T_f), corresponding to the maximum in $\chi'(T)$ and to the increase in $\chi''(T)$, the thermal energy is not enough to allow the magnetization of these systems to follow the ac field.

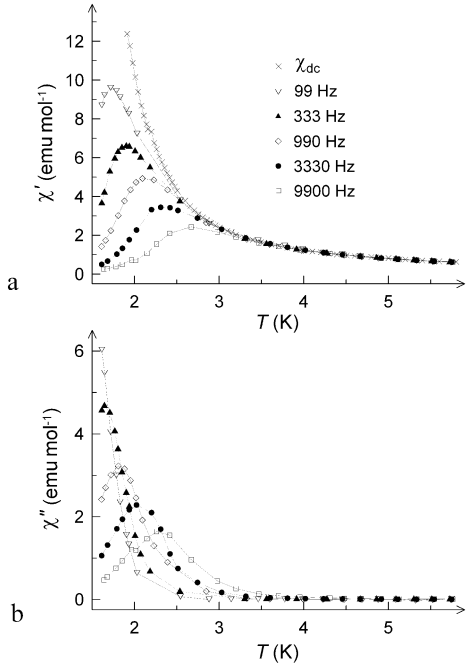

Figure 10. (a) χ' Temperature dependences at different frequencies of the ac field for **2**; (b) χ'' temperature dependence.

In these types of materials, the χ_{ac} frequency (ω) dependence is usually characterized through the parameter $\psi = \Delta T_f/[T_f\Delta(\log\omega)]$ and a value of $\psi = 0.23$ was obtained for **2**. This value is much larger than that observed for spin-glass-like materials ($\psi \approx 0.01$) but comparable to that observed in other materials such as SP, SMM, SCM, or highly frustrated magnets ($\psi \approx 0.1$), or even in cluster glasses (CG), which exhibit values of ψ ranging from ca. 0.01 to 0.1.

The magnetization relaxation was probed in the temperature range from 1.6 to 3.8 K. At fixed temperatures, χ' and χ'' were measured while the ω was varied from 1 Hz to 10 kHz. These data provided Cole–Cole plots (χ'' vs. χ' plots) as the one obtained at 1.6 K, shown in Figure 11a. These results show good agreement with the generalized Debye model,[24] $\chi(\omega) = \chi_S+(\chi_T+\chi_S)/(1+i\omega\tau)^{1-\alpha}$, where χ_S is the adiabatic susceptibility, χ_T is the isothermal susceptibility, τ is the average magnetization relaxation time, and α is a parameter that ranges from 0 to 1 and quantifies the width of the relaxation time distribution ($\alpha = 0$ corresponds to the ideal Debye model,[24] with a single relaxation time). The fit obtained at 1.6 K is represented by the solid line in Figure 11a, giving the parameters of $\chi_S = 0.09$ emu mol^{-1}, $\chi_T = 23.08$ emu mol^{-1}, $\alpha = 0.170$, $\tau = 0.00143$ s.

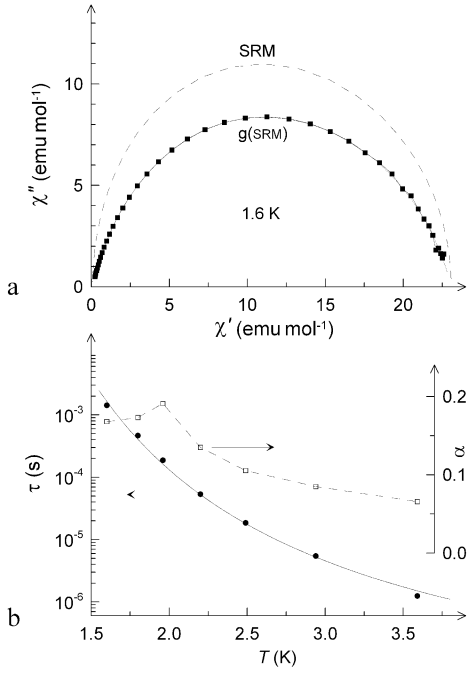

Figure 11. (a) Cole–Cole plots for **2** at 1.6 K. The dashed and solid lines correspond to a single relaxation model (SRM) and to a distribution of single relaxation modes [g(SRM)] for $T = 1.6$ K (see text); (b) temperature dependence of the parameters τ (squares/left scale) and α (circles/right scale).

The temperature dependence of the parameters τ and α is shown in Figure 11b. The relaxation times [$\tau(T)$] follow the Arrhenius law, $\tau(T) = \tau_0\exp(E_b/k_BT)$, where the preexponential factor $\tau_0 = 5.43\times10^{-9}$ s and the energy barrier for the relaxation of the magnetization $E_b = 20.20$ K. The parameter α shows an increase upon warming, a maximum at 2 K, and decreases at higher temperatures as expected for a system approaching paramagnetic behavior. The small α values obtained, along with the nearly semicircular and symmetrical shape of the Cole–Cole plots, are consistent with only one single magnetization relaxation process with a narrow distribution of the relaxation times.

In the spin freezing of compound **2**, unlike in spin-glasses, CG, and SP, the application of a magnetic field ($H > 100$ G) increases T_f and strongly suppresses $\chi'(T)$ for all

temperatures below T_f (Figure S4 in the Supporting Information). A similar effect was observed for the frustrated magnet $Dy_2Ti_2O_7$.[23a]

The nonlinear ac susceptibility temperature dependence of **2**, obtained with an ac field of 5 G and at a frequency of 300 Hz, is shown in Figure 12. Peaks in both the second (χ_2) and third (χ_3) harmonics were observed. The peak in χ_3 is consistent with the occurrence of a magnetic phase transition and the peak in χ_2 indicates the presence of a spontaneous magnetization.[25]

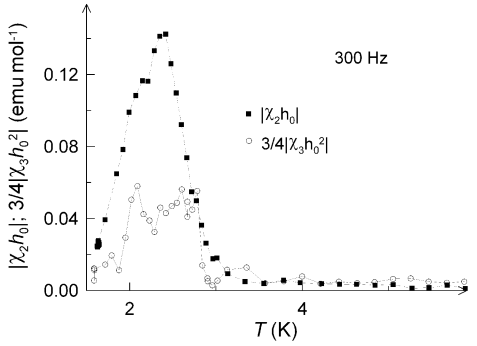

Figure 12. Nonlinear susceptibilities $|\chi_2 h_0|$ and $3/4|\chi_3 h_0^2|$ temperature dependence of **2**, with an ac field of 5 G (zero applied dc field) at ω = 300 Hz.

The above-described magnetic properties of compound **2**, namely, the magnetization relaxation, are inconsistent with spin-glass or SP behaviors. In addition, the crystal structure of this compound, although not determined, is similar to that of **3**, and it rules out possibilities of SMM and SCM. The absence of a maximum in the ZFC magnetization typical of CG, as well as in other slow relaxation materials, was not observed in **2**. It is possible to observe consistent similarities of the magnetic behavior of **2** with those of highly frustrated magnets, such as the pyrochlore compound $Dy_2Ti_2O_7$, which belongs to a class of frustrated magnets often referred to as "spin-ice" magnets.[23] For a long time, only AFM materials were considered to give rise to frustration; however, the discovery of the topological frustrated ferromagnets (spin-ice magnets) extended the geometric frustration to FM materials as well. In this class of compounds, despite the fact that the spins reside on a periodic lattice, they are so frustrated that they freeze in a random state instead of undergoing long-range order.

Assuming that **2** has a similar crystal structure to that of compound **3**, as indicated by the similar powder X-ray diffraction pattern, the magnetic frustration of **2** can be explained by the peculiar perpendicular arrangement of the chains in the adjacent layers combined with the magnetic anisotropy of the $[Mn(Cp^*)_2]^+$ cations. This leads to a situation where, in the absence of an applied magnetic field, it is possible to consider four nearly degenerated configurations from the spins in two interacting chains in adjacent layers, corresponding to the ground state, which are schematically represented in Figure 13. In the same way as in the spin-ice magnets, the degeneracy of the ground state in compound **2** must lead to a situation where upon cooling the system freezes in a random state. Then, the magnetic moments in adjacent FM coupled chain layers can present any of the four arrangements presented in Figure 13. Thus, the magnetic system does not achieve long-range order, and as in the case of the pyrochlore compounds at low temperatures, **2** becomes a frustrated magnet.

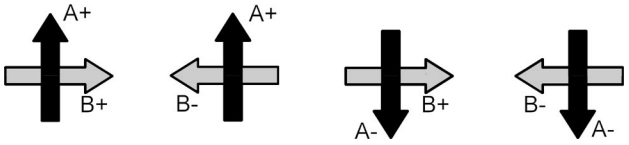

Figure 13. Possible arrangements of two chains in adjacent layers for compound **2** in the absence of an applied magnetic field.

Considering the crystal structure of these CT salts and the cation magnetic anisotropy in compound **2**, it is reasonable to expect that two of the above-mentioned four configurations (Figure 13) can have a smaller energy, because the cations are considerably tilted in relation to the chain axis (and thus, the individual moments of the molecules are expected to be out of plane with a nonnegligible component in the perpendicular direction to the chain layers). In this sense, depending on the cooling rate a larger number of pairs of layers with configurations corresponding to the lower energy state must be present at low temperatures. Furthermore, the effect of impurities and defects cannot be neglected in this ordering process, as its presence could lead to the fragmentation of the FM chains. Then, with cooling, domain wall arrangements of the broken chains could gradually freeze and give rise to a disordered 3D arrangement of FM coupled chain segments.

Magnetic Behavior of [Cr(Cp)$_2$][Ni(α-tpdt)$_2$] (3)*

For compound **3**, the magnetization isothermal obtained at 1.7 K is shown in Figure 14, and its behavior resembles that observed for CT salt **2**. At low magnetic fields, the magnetization increases faster than the Brillouin function (solid line) and for higher fields ($H > 10$ kG) the magnetization increase becomes more gradual and is not saturated even at fields as high as 120 kG, where it attains a value of ca. 3.6 $N\mu_B$, which is lower than the calculated saturation magnetization (4 $N\mu_B$) for S_A = 1/2, S_D = 3/2, g_A = 2.06,[2] and g_D = 2.0.[7]

Down to 1.65 K, no magnetic ordering was detected in compound **3**, which is attributed to weaker magnetic intermolecular coupling and to the lack of magnetic anisotropy in the $[Cr(Cp^*)_2]^+$ cation. However, in the absence of an external applied magnetic field, the ac susceptibility measurements show a clear increase in χ' below 10 K, which indicates the onset of an ordering process that may correspond to either an AFM transition (as in **1**) or spin-freezing (as in **2**).

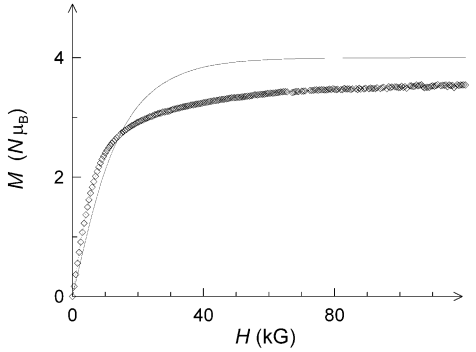

Figure 14. Magnetization field dependence at 1.7 K for **3**; the solid line represents the calculated values from the Brillouin function.

Conclusions

Following the report of the metamagnet [Fe(Cp*)$_2$][Ni(α-tpdt)$_2$],[2] two new CT salts based on [M(Cp*)$_2$]$^+$ cations (D$^+$) (M = Mn and Cr) and on the [Ni(α-tpdt)$_2$]$^-$ anion (A$^-$) were prepared and characterized in comparison with the M = Fe analogue. The crystal structures of the three compounds are similar and consist of alternating layers composed of parallel mixed chains (···D$^+$A$^-$D$^+$A$^-$D$^+$A$^-$···), where the chains in adjacent layers show perpendicular arrangement. The magnetic behavior of the series [M(Cp*)$_2$][Ni(α-tpdt)$_2$] with Fe (**1**), Mn (**2**) and Cr (**3**) was characterized by dc magnetization and ac susceptibility measurements.

At high temperatures, these salts exhibit similar magnetic behaviors dominated by ferromagnetic (FM) interactions. However, they reveal quite distinct magnetic behaviors at low temperatures. Compound **1** shows an AFM ground state (T_N = 2.5 K) and a metamagnetic behavior, compound **2** is a frustrated magnet with a blocking temperature of ca. 4 K, and compound **3** remains a paramagnetic down to 1.65 K.

The magnetic behavior of these salts is fairly well explained by the McConnell I model. According to this model, the dominant FM interactions are assigned to D$^+$A$^-$ intrachain contacts. Furthermore, this mechanism indicates that these strong FM interactions coexist with weaker AFM interactions associated with intralayer interchain D$^+$A$^-$ contacts as well as with D$^+$D$^+$ and A$^-$A$^-$ interlayer contacts. This magnetic anisotropy seems to be in good agreement with the metamagnetic behavior exhibited by **1**. The distinct magnetic ordering of compounds **1** and **2** is attributed to weaker AFM interchain intralayer coupling, or even to a FM interchain coupling induced by the A$^-$A$^-$ intralayer contacts in the case of **2**. This leads to an AFM intralayer interchain arrangement in **1**, but seems to favor a FM alignment in the case of **2**. These factors combined with the perpendicular arrangement of the chains in adjacent layers and the magnetic anisotropy of the cations lead to a degenerate ground state and to frustrated magnet behavior in compound **2**.

The absence of magnetic ordering in CT salt **3** is attributed to weaker magnetic coupling and to the lack of magnetic anisotropy from the cation.

Experimental Section

General Remarks: All manipulations were carried out with exclusions of air under a nitrogen atmosphere, unless stated otherwise. The starting ketone, 5,6-thieno[2,3-*d*]-1,3-dithiol-2-one,[1] the tetrabutylammonium salt of nickel(III) bis(2,3-thiophenedithiolate),[2] [Mn(Cp*)$_2$]PF$_6$,[6] and [Cr(Cp*)$_2$]PF$_6$,[7] were prepared following the methods previously reported. All solvents were purified following standard procedures. Other chemicals were commercially obtained and used without any further purification.

[Cr(Cp*)$_2$][Ni(α-tpdt)$_2$] (3): A solution of [Cr(Cp*)$_2$]PF$_6$ (24 mg, 5×10^{-5} mol) in acetonitrile (2 mL) was slowly added to a solution of *n*Bu$_4$N[Ni(α-tpdt)2] (30 mg, 5×10^{-5} mol) in acetonitrile (3.5 mL) under an inert atmosphere without stirring. After a few hours, dark-green crystals precipitated. Yield: 24 mg {70% based on *n*Bu$_4$N[Ni(α-tpdt)$_2$]}. $C_{28}H_{34}CrNiS_6$ (673.63): calcd. C 49.92, H 5.08, S 28.56; found C 48.87, H 4.98, S 27.78.

[Mn(Cp*)2][Ni(α-tpdt)2] (2): Prepared by following the method used to prepare **3** but with the use of [Mn(Cp*)$_2$]PF$_6$ instead of [Cr(Cp*)$_2$]PF$_6$. Dark-green microcrystalline powder. Yield: 20 mg {60% based on *n*Bu$_4$N[Ni(α-tpdt)$_2$}. $C_{28}H_{34}MnNiS_6$ (676.57): calcd. C 49.71, H 5.06, S 28.43; found C 49.98, H 4.99, S 29.21.

Magnetic Measurements: Measurements were performed by using a longitudinal Faraday system (Oxford Instruments) with a 70 kG superconducting magnet for static measurements in the range 1.7–300 K; a Quantum Design SQUID (MPS) magnetometer, with a 55 kG superconducting magnet in the range 1.8–300 K; and a Maglab 2000 system (Oxford Instruments), for dc magnetization and ac susceptibility under fields up to 120 kG down to a lower temperature limit of 1.5 K. The Faraday system was used with a magnetic fields of 2–5 T and forward and reverse gradients of field of 5kG G cm^{-1}. A polycrystalline sample (10–15 mg) was placed inside a previously calibrated thin-wall Teflon bucket. The force was measured with a microbalance (Sartorius S3D-V). The Maglab 2000 system was used for magnetization measurements of similar polycrystalline samples (in gelatin capsules) at different magnetic fields by using an extraction technique and for ac susceptibility measurements by using a typical ac field of 1 G. The SQUID magnetometer was used particularly to measure the magnetization temperature dependence at low fields (5–200 G).

X-ray Crystallographic Study: Crystal data and details of the refinement parameters for [Cr(Cp*)$_2$][Ni(α-tpdt)$_2$] are summarized in Table 3. X-ray diffraction experiments were performed with an Enraf–Nonius CAD-4 diffractometer by using graphite-monochromized Mo-K_α radiation (λ = 0:71073 Å). A semiempirical absorption correction based on ψ-scan was applied.[26] The structure was solved by direct methods by using SIR97[27] and refined by full-matrix least-squares methods on F^2 by using the program SHELXL97[28] and the winGX software package.[29] All non-hydrogen atoms were refined anisotropically. Cp* H atoms were treated as riding, with C–H 0.96 Å and U_{iso} = 1.5 U_{eq}(C). The remaining H atoms were treated as riding with C–H 0.93 Å and U_{iso} = 1.2 U_{eq}(C). Graphical representations were prepared by using SCHAKAL 97.[30]

Table 3. Crystal data and experimental details for $[Cr(Cp^*)_2][Ni(\alpha\text{-tpdt})_2]$.

	$[Cr(Cp^*)_2][Ni(\alpha\text{-tpdt})_2]$
Empirical formula	$C_{28}H_{34}CrNiS_6$
Formula weight	673.62
Temperature (K)	243(2)
Wavelength (Å)	0.71069
Crystal system; space group	Monoclinic; $P2_1/c$
a (Å)	10.046(3)
b (Å)	10.270(3)
c (Å)	15.528(3)
β (°)	104.88(2)
Volume (Å^3)	1548.3(7)
Z; Calculated density (Mg m^{-3})	2; 1.445
Absorption coefficient (mm^{-1})	1.380
$F(000)$	700
Crystal size (mm^3)	$0.40 \times 0.30 \times 0.24$
θ range for data collection (°)	2.10 to 25.98
Index ranges	$-12 \le h \le 0$; $0 \le k \le 12$; $-18 \le l \le 19$
Reflections collected/unique	3055/2897 [R(int) = 0.1001]
Completeness to θ = 25.98°	95.2%
Max. and min. transmission	0.7390 and 0.6178
GOF on F^2	1.039
Final R indexes [$I > 2\sigma(I)$]	R_1 = 0.0682; wR_2 = 0.1678
R indexes (all data)	R_1 = 0.1122, wR_2 = 0.1928
Largest diff. peak and hole (e Å^{-3})	0.703 and –0.764

CCDC-615973 contains the supplementary crystallographic data for this paper. These data can be obtained free of charge from The Cambridge Crystallographic Data Centre via www.ccdc.cam.ac.uk/data_request/cif.

Supporting Information (see footnote on the first page of this article): Intrachain arrangements of CT salts **1** and **3**; interlayer A$^-$A$^-$ contacts of **1**; isofield and isothermal magnetization measurements of **1**; χ' temperature dependence for various values of the applied dc field for **2**.

Acknowledgments

This work was partially supported by the Fundação para a Ciência e Tecnologia (Portugal) (contract POCTI/35342/QUI/2000 and POCTI/QUI/45108/2002), the DGI Spain (projects CTQ2006-06333/BQU, BQU2002-04587-C02-02, and UNBA05-33-001), the DGR Catalonia (projects 2005SGR-00591, 2001SGR-0044, and 2005-PEIR-0051/69), and the Instituto Carlos III, MIyC, through "Acciones CIBER" Ciber BBN. The collaboration between the team members of Sacavém and Barcelona was supported under the CSIC-ICCTI bilateral agreement. This work also benefited from COST action D35 and MAGMANet Network of Excellence.

[1] D. Belo, H. Alves, E. B. Lopes, M. T. Duarte, V. Gama, R. T. Henriques, M. Almeida, A. Pérez-Benítez, C. Rovira, J. Veciana, *Chem. Eur. J.* **2001**, *7*, 511–519.
[2] D. Belo, H. Alves, S. Rabaça, L. C. Pereira, M. T. Duarte, V. Gama, R. T. Henriques, M. Almeida, E. Ribera, C. Rovira, J. Veciana, *Eur. J. Inorg. Chem.* **2001**, 3127–3132.
[3] D. Belo, M. J. Figueira, J. Mendonça, I. C. Santos, M. Almeida, R. T. Henriques, M. T. Duarte, C. Rovira, J. Veciana, *Eur. J. Inorg. Chem.* **2005**, 3337–3345.
[4] D. Belo, M. J. Figueira, J. P. M. Nunes, I. C. Santos, L. C. Pereira, V. Gama, R. T. Henriques, M. Almeida, C. Rovira, *J. Mater. Chem.* **2006**, *16*, 2746–2756.
[5] H. M. McConnell, *J. Chem. Phys.* **1963**, *39*, 1910.
[6] J. L. Robbins, N. M. Edselstein, S. R. Cooper, J. C. Smart, *J. Am. Chem. Soc.* **1979**, *101*, 3853–3857.
[7] J. J. L. Robbins, N. Edelstein, B. Spencer, J. C. Smart, *J. Am. Chem. Soc.* **1982**, *104*, 1882–1893.
[8] W. E. Broderick, J. A. Thompson, M. R. Godfrey, M. Sabat, B. M. Hoffman, *J. Am. Chem. Soc.* **1989**, *111*, 7656–7657.
[9] C. Mahadevan, M. Seshasayer, P. Kuppusamy, P. T. Manoharan, *J. Cryst. Spectrosc. Res.* **1985**, *15*, 305–316.
[10] M. Deumal, J. J. Novoa, M. J. Beapark, P. Celani, M. Olivucci, M. A. Robb, *J. Phys. Chem. A* **1998**, *102*, 8404–8412.
[11] M. Deumal, J. Cirujeda, J. Veciana, J. J. Novoa, *Chem. Eur. J.* **1999**, *5*, 1631–1642.
[12] S. Rabaça, R. Meira, L. C. J. Pereira, M. T. Duarte, J. J. Novoa, V. Gama, *Inorg. Chim. Acta* **2001**, *326*, 89–100.
[13] a) J. Blumel, N. Hebendaz, P. Hudeczek, F. H. Kohler, W. Strauss, *J. Am. Chem. Soc.* **1992**, *114*, 4223–4230; b) C. Kollmar, O. Kahn, *J. Chem. Phys.* **1992**, *96*, 2988–2997; c) H. Heise, F. H. Köhler, M. Herker, W. Hiller, *J. Am. Chem. Soc.* **2002**, *124*, 10823–10832.
[14] J. Scweitzer, A. Bencini, C. Carbonera, A. J. Epstein, S. Golhen, E. Lelièvre-Berna, J. S. Miller, L. Ouahab, Y. Pontillon, E. Ressouche, A. Zheludev, *Polyhedron* **2001**, *20*, 1771–1778.
[15] A. D. Becke, *J. Chem. Phys.* **1993**, *98*, 5648–5652.
[16] P. J. Hay, W. R. Wadt, *J. Chem. Phys.* **1985**, *82*, 270–283.
[17] a) V. Gama, M. Teresa Duarte in *Magnetism: Molecules to Materials V* (Eds.: J. S. Miller, M. Drillon), Wiley-VCH, Weinheim, **2005**, pp. 1–40; b) V. Gama, D. Belo, S. Rabaça, I. C. Santos, H. Alves, J. C. Waerenborgh, M. T. Duarte, R. T. Henriques, *Eur. J. Inorg. Chem.* **2000**, 2101–2110; c) W. E. Broderick, J. A. Thompson, B. M. Hoffman, *Inorg. Chem.* **1991**, *30*, 2958–2960; d) S. Rabaça, B. J. C. Vieira, R. Meira, I. C. Santos, L. C. J. Pereira, M. T. Duarte, V. Gama, *Eur. J. Inorg. Chem.*, DOI: 10.1002/ejic.200800380.
[18] D. Belo, L. C. J. Pereira, M. Almeida, R. T. Henriques, J. J. Novoa, C. Rovira, J. Veciana, V. Gama, manuscript in preparation.
[19] a) J. A. Mydosh, *Spin Glasses: An Experimental Introduction*, Taylor & Francis, London, **1993**; b) A. P. Young, *Rev. Mod. Phys.* **1986**, *58*, 801; c) M. A. Gîrtu, M. Wynn, K.-I. Sugiura, J. S. Miller, A. J. Epstein, *J. Appl. Phys.* **1997**, *81*, 4410–4412; d) S. J. Etzkorn, W. Hibbs, J. S. Miller, A. J. Epstein, *Polyhedron* **2003**, *22*, 1751–1754; e) S. J. Etzkorn, *Magnetic Relaxation in Organic-Based Magnets*, Ph. D. Thesis, The Ohio State University, **2003**; f) M. Balanda, K. Falk, K. Griesar, Z. Tomkowicz, W. Haase, *J. Magn. Magn. Mater.* **1999**, *205*, 14–26.
[20] a) A. H. Morrish, *The Physical Principles of Magnetism*, Wiley, New York, 1**965**; b) F. Palacio, *Molecular Magnetism: From Molecular Assemblies to the Devices* (Eds.: E. Coronado, P. Delhaès, D. Gatteschi, J. S. Miller), Kluwer Academic Publishers, Boston, **1996**, p. 5.
[21] a) H. Oshio, M. Nihei, A. Yoshida, H. Nojiri, M. Nakano, A. Yamaguchi, Y. Karaki, H. Ishimoto, *Chem. Eur. J.* **2005**, *11*, 843–848 and references cited therein; b) H. Miyasaka, T. Nezu, K. Sugimoto, K. Sugiuara, M. Yamashita, R. Clérac, *Chem. Eur. J.* **2005**, *11*, 1592–1602 and references cited therein; c) D. Gatteschi, R. Sessoli, *Angew. Chem. Int. Ed.* **2003**, *42*, 268–297.
[22] a) R. Clérac, H. Miyasaka, M. Yamashita, C. Coulon, *J. Am. Chem. Soc.* **2002**, *124*, 12837–12844; b) L. Bogani, C. Sangregorio, R. Sessoli, D. Gateschi, *Angew. Chem. Int. Ed.* **2005**, *44*, 5817–5821 and references cited therein; c) H. Miyasaka, R. Clérac, K. Mizushima, K. Sugiura, M. Yamashita, W. Wernsdorfer, C. Coulon, *Inorg. Chem.* **2003**, *42*, 8203–8213 and references cited therein.
[23] a) J. Snyder, J. S. Slusky, R. J. Cava, P. Schiffer, *Nature* **2001**, *413*, 48–51 and references cited therein; b) S. T. Bramwell,

M. J. P. Gingras, *Science* **2001**, *294*, 1495–1501 and references cited therein.

[24] a) K. S. Cole, R. H. Cole, *J. Chem. Phys.* **1941**, *9*, 341; b) S. M. J. Aubin, Z. Sun, L. Pardi, J. Krzystek, K. Folting, L. C. Brunel, A. L. Rheingold, G. Christou, D. N. Hendrickson, *Inorg. Chem.* **1999**, *38*, 5329–5340.

[25] a) M. Balanda, T. Korzeniak, R. Pelka, R. Podgajny, M. Rams, B. Sieklucka, T. Wasiutynski, *Sol. State Sci.* **2005**, *7*, 1113–1124; b) S. Mukherjee, R. Ranganathan, S. B. Roy, *Phys. Rev. B* **1994**, *50*, 1084–1089.

[26] A. C. T. North, D. C. Phillips, F. S. Mathews, *Acta Crystallogr., Sect. A* **1968**, *24*, 351.

[27] A. Altomare, M. C. Burla, M. Camalli, G. Cascarano, G. Giacovazzo, A. Guagliardi, A. G. G. Moliterni, G. Polidori, R. Spagna, *J. Appl. Crystallogr.* **1999**, *32*, 115.

[28] G. M. Sheldrick, *SHELXL97: Program for Crystal Structure Refinement*, University of Göttingen, Germany, **1997**.

[29] The winGX software package: L. J. Farrugia, *J. Appl. Crystallogr.* **1999**, *32*, 837–838.

[30] E. Keller, *J. Appl. Crystallogr.* **1989**, *22*, 19–22.

Received: June 18, 2008
Published Online: ■

Magnetic Anisotropy

$[M(Cp^*)_2][Ni(\alpha\text{-tpdt})_2]$ [M = Fe (**1**), Mn (**2**), Cr (**3**)] show similar multilayer structural arrangements, but at low temperatures, **1** is a metamagnet, **2** is a frustrated magnet, and **3** is a paramagnet. The unusual behavior of **2** is due to a degenerate ground state resulting from interlayer chain arrangements and magnetic anisotropy.

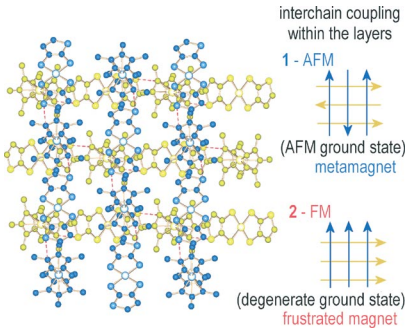

Keywords: Donor–acceptor systems / Metallocenes / S ligands / Through-space interactions / Magnetic anisotropy

